Engineered Science
DOI: https://dx.doi.org/10.30919/es1389

Embedded Copper Foam Effect on the Nanofluids Thermal Cooling Performance of the Electric Vehicle Battery Pack

S. Poojeera,[1] P. Vengsungnle,[2] J. Jongpluempiti,[2] S. Eiamsa-ard,[3] N. Naphon,[4] A. Srichat,[5] K. Manatura[6] and P. Naphon[7,*]

Abstract

Power packs generate complex heat while used, significantly affecting thermal performance and lifetime energy storage devices. For this reason, thermal cooling is essential to the system functioning. Improving heat management systems is crucial for fully using electric mobility as electric vehicle technology progresses. Flowing a ferrofluid cooling system via a channel flow channel integrated with the copper foam sheet has been performed. This study continuously employed numerical analysis and experimental data to estimate the battery pack temperature distribution. Aluminum cooling channels, some with and without copper foam sheets, comprise the battery module. The research examined the pack, which has twelve prismatic cells with a combined current of 50A and a voltage of 38.4V. The surface area increases when the flow channel containing the copper foam sheet experiences increased turbulence. With increasing porosity, a copper foam structure experiences a more significant heat transfer enhancement and inertial drag due to separation flow. Therefore, cooling performance without copper foam is compared with those with copper foam. For the none-porous media with channel width = 2 mm (NPM_CW2mm), the hottest temperature is 32 °C; for NPM_CW1mm, it is 30.2 °C; and for PM_CW1mm, it is 29.4 °C. However, many relevant parameters are significant to the cooling performance of the cooling pack with copper foam, and this must be continuously studied. These results are relevant to developing the battery thermal management system as they investigate various methods to improve thermal cooling and heat transfer to achieve stable and safe operation.

Keywords: Copper foam sheet; Nanofluids; Thermal cooling; Electric vehicle battery pack.
Received: 11 December 2024; Revised: 07 January 2025; Accepted: 19 January 2025.
Article type: Research article.

1. Introduction

Using a coolant medium, which transmits heat into the cooling system, is essential for temperature management in packs and preventing overheating in any given situation. A coolant, a kind of heat transfer cooling medium, has cheap viscosity, big thermal capacity, non-toxicity, and cheap cost—those are the ideal properties of a coolant medium. Fig. 1 shows the battery thermal cooling system with different coolant mediums.

[1] *Department of Mechanical Engineering, Faculty of Engineering, Rajamangala University of Technology Isan, Khon Kaen Campus, 40000, Thailand*
[2] *Department of Agricultural Machinery Engineering, Faculty of Engineering and Architecture, Rajamangala University of Technology Isan, Nakhonratchasima, 30000, Thailand*
[3] *Department of Mechanical Engineering, Faculty of Engineering and Architecture, Rajamangala University of Technology Suvarnabhumi, Phranakhon Si Ayutthaya, 13000, Thailand*
[4] *Department of Pharmaceutical Chemistry, Faculty of Pharmacy, Srinakharinwirot University, 63 Rangsit-Nakhornnayok Rd., Ongkharak, Nakhorn-Nayok, 26120, Thailand*

1.1 An air-cooling method

The easiest and least expensive option is to use air as a heat transfer medium; however, liquid cooling provides better results. Forced convection, by means such as piping in cooled air or just blowing outside air over the cells, removes the heat that the battery produces. The drawbacks include a cooling air flow rate of only 100–250 m^3/h, a lack of efficiency, noise, an uneven distribution of temperatures inside the batteries, the possibility of fouling, and safety issues caused by the release of harmful gases from the battery pack. Air cooling systems have been extensively studied and used in commercial applications due to their status as one of the most prevalent and traditional strategies, as shown in Fig. 2. Both free and forced air cooling are the main types of air-based battery cooling. There is a significant operational difference between the two methods. When using the passive method, the coolant is forced directly into the pack from the surrounding environment without any other devices; in contrast, active air cooling involves forcing air into the battery pack using a fan or other device. The use of heating, ventilating, and air conditioning systems in commercial environments has been

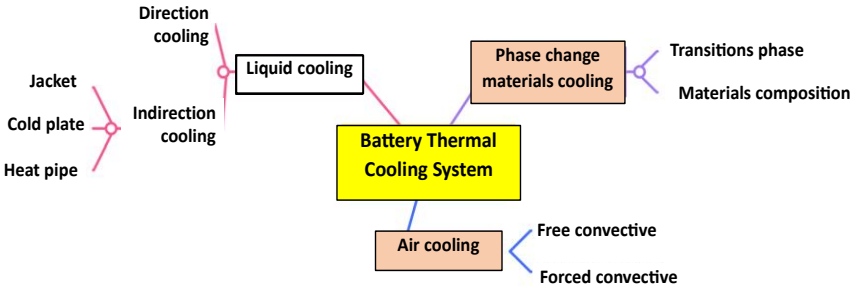

Fig. 1: Summary of each of the battery thermal management systems (BTMSs).

the subject of much research.[1,2] One air-based battery cooling uses natural air cooling, while the other uses forced air cooling.[3,4] A battery pack may be "cooled" via active airflow or "passively" by drawing air straight from the surrounding environment, depending on your preference.[5,6] Air cooling is a popular choice among automotive manufacturers for battery temperature control systems due to its simplicity, low energy requirement, cheap cost, and excellent design. Much research has focused on BTMS, which functions in the air.[7-12] Alharbi *et al*.[13] designed the battery within the pack to improve BTMS air-based.

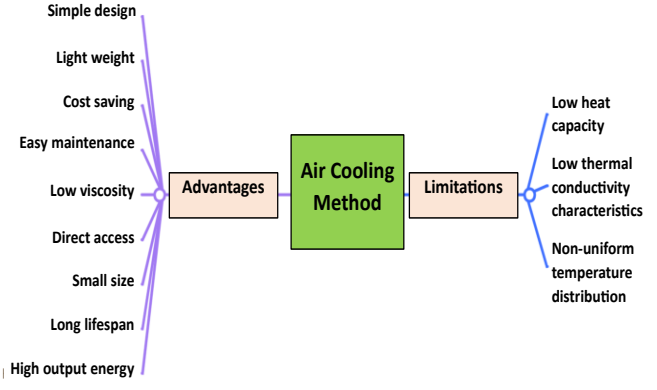

Fig. 2: Summary of air-cooling method advantages and disadvantages.

After conducting quantitative analysis on a pack with three different battery designs—rectangle, lozenge, and triangle—they compared the pressure drop and temperature contour findings. Chen *et al*.[14] introduced the "U-shape" flow analysis to improve battery pack cooling. Findings show that the suggested layout reduced cooling fan power usage by 32% and cell temperature differential by 70%. Using quantitative approaches, Liu and Zhang suggested new airflow configurations.[15] Their findings showed that the U-shaped airflow route caused a temperature rise of 35.3%, the Z-shaped path of 46.6%, and the J-shaped manner of 31.1%. Over a decade, there has been little change in the optimization methods used for air cooling designs. The designs all optimize the same parameter characteristics, including the airflow path and layout, the geometry and inlet/outlet locations, and the configuration and arrangement of the batteries.[16,17] A high heat transfer coefficient, ease of installation, and low cost are some benefits of forced air conditioning. Nevertheless, more optimization strategies and precise alteration of the coolant medium's behavior are necessary for a longer driving range and faster charging.[18]

1.2 The liquid cooling method

The complexity of liquid cooling systems is higher than that of air-cooling systems. With a battery thermal management system that uses liquid cooling, the heat transfer from the battery to the coolant is accomplished by encasing the cells in a jacket that transfers heat from a heated liquid or cooled plate to the surface of the cells or by immersing the cells in a dielectric fluid. Cooling media such as water, ethylene glycol, or refrigerants may be used in liquid cooling systems that employ a non-direct contact technique. However, in order to prevent short circuits, the liquid used in the direct contact approach must be a dielectric, such as mineral oils or silicone-based liquids. Direct liquid cooling over an air-cooled system has many benefits, including a higher cooling rate, more uniform cell temperatures, and reduced overall system size. The cooling system can only run on an available power source with direct liquid cooling, and the thermal management system cannot include heating, which is necessary for ambient temperatures below 0 °C.

Compared to air cooling, the indirect-contact liquid cooling technology has better cooling performance, allows for heating integration, and is easy to maintain, among other benefits. On the other side, it requires more room and weighs more overall, which drives up the price since auxiliary components like a chiller and heat sink are required, and it has much inertia because of how hot it is. Fig. 3 shows the advantages and disadvantages of the liquid cooling method. Direct and indirect contact may transfer heat from the cooling

[5] *Department of Mechanical Engineering, Faculty of Technology and Engineering, Udon Thani Rajabhat University, Udon Thani, 41000, Thailand*
[6] *Department of Mechatronics Engineering, Faculty of Engineering and Technology, Rajamangala University of Technology Isan, Nakhon Ratchasima, 30000, Thailand*
[7] *Department of Mechanical Engineering, Faculty of Engineering, Srinakharinwirot University, 63 Rangsit-Nakhornnayok Rd., Ongkharak, Nakhorn-Nayok, 26120, Thailand*
**Email:* paisarnn@g.swu.ac.th (P. Naphon)

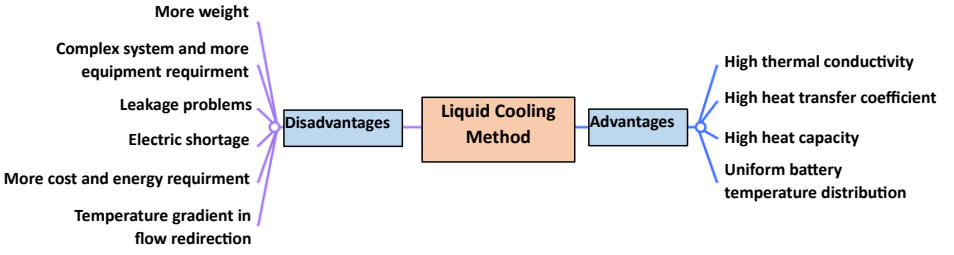

Fig. 3: Summary of advantages and disadvantages of the liquid cooling method.

media to the battery cells. Dielectric liquids with desirable properties, such as low toxicity, non-flammability, high thermal stability, and high heat transfer coefficient, are often used in the direct contact approach, which entails immersing the battery cells in them. It typically ensures temperature distribution throughout the power battery pack cell surfaces. Dielectric fluids are often found in various substances, such as mineral oils, perfluoroalkanes, deionized water, fluorocarbons, and silicone-based fluids.[19] Most coolant studies center on four main categories: nanofluids, liquid metals, water, and oil. Prioritizing the optimization of coolant type, temperature, flow rate, shape, pressure loss, leakage, and channel designs is paramount when building a liquid cooling system.[20-24] Deng *et al*.[25] compared mineral oil and water-glycol coolants using the same channel widths and flow rates. The findings indicate that oil is superior to water glycol for cooling purposes.

Additionally, they found that mineral oil had better heat transfer efficiency than air coolants, likely due to its high thermal conductivity. Several environmental factors may enhance the cooling effectiveness of silicone transformer fluid coolant, as shown in a study by Nelson *et al*.[26] Water/glycol coolant, with its large heat capacity, may effectively lower the most significant temperature difference compared to conventional coolants. Improved thermal conductivity is a property of coolant fluids that include metal particles. Yang *et al*.[27] investigated parallel liquid BTMS from a mathematical and practical perspective for prismatic battery packs. Improved cooling resulted from a more extensive intake mass flow rate and more inputs and outputs. Wang *et al*.[28] improved the method of liquid cooling by using silica plates. The goal was to increase the cooling plate efficiency; therefore, they attached a thermal silica plate. In contrast, microchannel cooling reduces heat transfer at the coolant fluid departure point. A small group of academics proposed placing roughed-up components into narrow channels based on their investigation into various optimization techniques. Guo *et al*.[29] studied the impact of inserting different styles of pin fins into small cooling channels on cooling performance. Cooling performance was good with the vertically placed square pin fins. Incorporating nanoparticles into liquid coolants improves their thermal performance, according to scientists.

Prior research indicates that water coolants outperform oil ones. Without an obstruction, the water coolant cannot transfer heat. Therefore, adding the correct quantity of nanoparticles is essential for improving cooling performance. Overweight leaks are a concern in the system, and construction is still an issue. The pressure loss from the channels is still there, even if the system is lighter and smaller, thanks to the compact channel cooling plates. New research on the liquid cooling mechanism may be necessary. Most of the battery thermal cooling has been done by Naphon *et al*.[30-36] They applied the heat transfer enhancement techniques with liquid/nanofluid for cooling both cylindrical and prismatic battery packs; nanofluid cooling,[30] thermoelectric ferrofluid,[31] water/nanofluid pulsating flow cooling,[32] coolant flow direction,[33,34] and inversed-zigzag channel ferrofluid flows,[35] and different ferrofluid flow arrangements.[36]

1.3 The phase change material cooling method

Researchers looked deeper into passive cooling as a solution to the problems caused by traditional coolants, such as their large volume, high cost, high power consumption, and additional equipment requirements. Phase change material (PCM) was the first coolant to catch their eye for potential

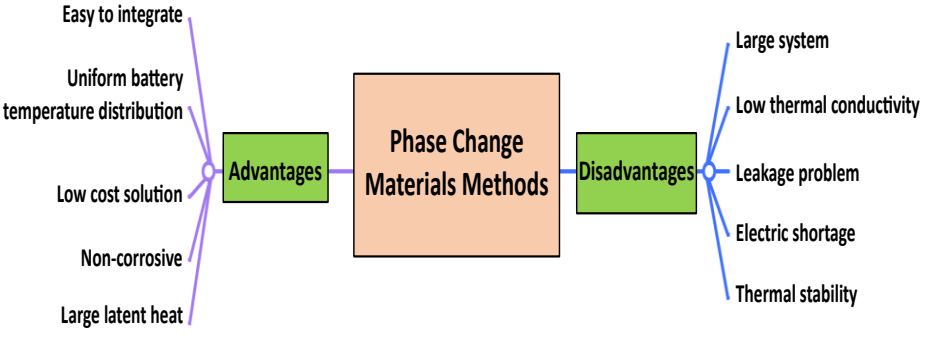

Fig. 4: Summary of advantages and disadvantages of the phase change material cooling method.

usage in various applications. A PCM is a material that, at a given temperature, may either absorb or release heat as it undergoes a phase shift, either melting or solidifying. Fluid-to-gas PCM and solid-to-liquid PCM are all examples of PCM. However, PCM has advantages and disadvantages, as shown in Fig. 4. Due to previous coolant issues, including bulk, cost, power needs, and additional equipment, researchers dug further into passive cooling.[37] They first became interested in PCM as a coolant for automobile use.[38] When a phase transition material melts or solidifies, it may either take heat from or provide heat to a system, depending on the temperature.[39,40] BTMS coolant mediums containing PCM have been the subject of increasing attention.[41,42] Battery cooling systems based on PCM demonstrated enhanced cooling efficiency and more uniform temperature distribution in a study by Wang *et al*.[43] A pack of graphene and PCM was used by Malik *et al*.[44] Mallow *et al*.[45] found that graphite foam wet with PCM improved charging behavior and thermal performance. Copper foam reduced PCM maximum temperature by 25% in an experiment by Rehman *et al*.[46] Additional research has shown that the conductivity and cooling efficacy of PCM may be improved by adding metal oxide,[47] metal fiber,[48] metal mesh,[49,50] and metal nanoparticles.[51] It would help if you considered how electrically conductive metals are to ensure a power battery is safe.[52] Thermoelectric cooling fins or sheets are only one of several potential improvements to the PCM-based BTMS that should be considered.[53,54] The dispersion of microscopic PCM particles into a fluid is one possible pathway for PCF sources.[55] As a thermal coolant, Wang *et al*.[56] used a phase-change nano-emulsion to compute and experimentally study the highest temperature. Some major drawbacks of passive cooling systems made of PCM materials are as follows. PCMs have a high melting point. The required battery cells must be heated to their melting points to use phase change characteristics, often exceeding 40 °C. Excessive heat shortens the life of the battery. As soon as the PCM's temperature drops below its melting point, the battery pack begins to heat up considerably. Poor thermal conductivity characterizes PCMs. Delays in heat dissipation or uneven distribution of heat might cause an explosion or damage to the pack.[57] The increase in the coolant thermal barrier leads to cold-pumped condensation cooling, which raises pack temperatures. Because of this, it is clear that PCM is insufficient as a cooling medium on its own and that other cooling media are necessary.

1.4 The combined cooling method

By using a hybrid coolant medium, BTMS blends many coolants mentioned before. According to the research, the coolant does not work as intended. They proposed using hybrid coolants to enhance the cooling efficiency, weight, volume, power, and cost of the BTMS.[58] However, after a while, the material begins to insulate. When heated above its melting point, its performance degrades. Use PCM in conjunction with active cooling to fix the previously stated problems. Following comparing PCM-only and PCM-filled mandrel systems, Zhao *et al*.[59] suggested a hybrid approach, using air-cooling BTMS with PCM cooling. According to Lazrak *et al*.[60] the temperature decreased by five degrees, and the uniform distribution varied by two degrees due to PCM and induced convection. Mehrabi-Kermani *et al*.[61] suggested combining PCM and copper foam to prolong the operating duration. The results demonstrated that copper foam quickly transferred heat, leading to a consistent distribution of temperatures because of its outstanding thermal conductivity. The liquid-based BTMS is very efficient at cooling but is bulky and needs specific components, which restricts its use. Rao *et al*.[62] used PCM coolant with a cooling system to develop a thermal model of hybrid batteries. According to the results, increasing the number of microchannels lowered the battery pack's maximum temperature. Liquid cooling with plate height, flow direction, flow velocity, battery gap, PCM melting point, and thermal conductivity were among the factors investigated by Bai *et al*.[63] The peak temperature increased by 4 ºC, and the temperature homogeneity decreased by 6 ºC due to the increased flow rate. In their innovative hybrid BTMS design, Akbarzadeh *et al*.[64] fused a PCM with a cooling plate. They investigated the proposed design using computational and experimental methods in several real-world contexts. They discovered that the hybrid cut used half as much electricity as the conventional cooling plate. Gou *et al*.[65] developed an innovative design for internal cooling by placing the heat pipe and PCM within the battery pack. With a hottest temperature of less than 31.5 ºC and a temperature differential of less than 1 degree Celsius, the suggested arrangement was effective. Jiang and Qu examined the cooling performance of a heat pipe and PCM system.[66] Their findings indicate that the heat pipe released the stored energy from the PCM and battery once the mixture hardened. One study by Zhang *et al*.[67] used a fan and PCM-soaked porous metal foam to study heat pipe-assisted BTMS. The study found that the temperature distribution was stable within 5 ºC. Adding an extra fan could significantly improve the results. In their research, Huang *et al*.[68] compared and contrasted two approaches for cooling battery packs. Trials involving temperature differences of 3 ºC or less were demonstrated. According to the author, heat pipes were crucial to the transmission process.

Operating the power pack of an energy storage device produces complicated heat, which has a major impact on the device's thermal performance and lifespan. Therefore, thermal cooling is critical for the system's proper operation. As mentioned above, many methods are used to cool the power pack. Understanding the variation of chemical phenomena, peak temperature, and temperature for operating conditions is vital. A battery cooling system could use various cooling approaches, each with its own set of pros and cons (see Figs. 2-4). Both the thermophysical characteristics of the coolant and the flow conditions affect its heat transferability. For the liquid cooling systems employ either water or oil. Many

people are interested in ferrofluid because of its potential use as a coolant in thermal devices that enhance heat transmission. Fluids with ferrofluid properties may improve heat transfer. A coolant medium must transfer heat to the cooling system for optimal temperature control in packs and complete protection against overheating. The ideal qualities of a coolant medium are low cost, non-toxicity, large thermal capacity, and low viscosity; a coolant is a kind of heat transfer cooling medium. Heat management system development is of utmost importance in fully using electric mobility as EV technology advances. This research continually used numerical analysis and experimental methods to run a ferrofluid cooling system via a channel flow channel embedded with the copper foam sheet to determine the battery pack temperature distribution. The calculated outcomes are confirmed by comparing them to the observed data.

2. Experimental apparatus and procedure

2.1. Experimental apparatus

As shown in Fig. 5, the battery unit is a present setup and insulated with an insulator (room temperature of 30 ºC, humidity ratio of 80%). The primary systems are a cooling loop, a refrigerated cooling system, a control system for charging and discharging, and an electrical control system. Following its chilling and regulation by the refrigeration cooling system, the coolant flows into the ultrasonic bath and storage tank before finally reaching the battery pack. After draining the reservoir, the coolant passes via the flowmeter and into the battery pack. The flowmeters measure the coolant flow rate, and the digital weight scale measures the fluid mass within 0.01% of the full-scale reading. Two type-T thermocouples measure the coolant temperatures within 0.1 percent of full scale at the battery pack inlet and outlet ports. The battery cell temperatures are measured using twelve thermocouples in three zones, including Zone L, M, and R, as seen in Fig. 6, pre-calibrated with a dry block type calibrator.

2.2 Ferrofluid preparation

The current study uses iron oxide nanoparticles (Fe_3O_4), the parameters of which are shown in Table 1. The ferrofluid was dispersed using an ultrasonic unit (DELTA) at very low concentrations (0.015 % by volume) since sticking in a flow channel was not an option. Once the ferrofluid is stable, it is stabilized by moving it about in the ultrasonic bath for an hour. Furthermore, the absorbance spectra of the nanofluids on the first and second days are measured using the spectrophotometer ultraviolet (UV)-1800. There was little change between the first and second days's % absorbance spectra, with an inaccuracy of just 1.03%, so it remains steady. For the whole experiment, the ultrasonic unit was maintained in On-mode for 20 minutes each hour to maintain the stable ferrofluid stationary condition. What follows is a determination of all ferrofluid parameters in Eqs. (1)-(4) based on the reported correlations.[69–72]

Table 1: Thermo-physical properties of water, Fe_3O_4.

Properties	Temperature (ºC)	Water	Fe_3O_4
Density, ρ (kg/m^3)	25±1	996.875	5180
Thermal conductivity, k (W/m.K)		0.60965	80.4
Viscosity, μ (mPa S)		0.7275	-
Specific heat,C_p (J/kg.K)		4181	670
Purity, %		-	>99.9
Average diameter, nm		-	23

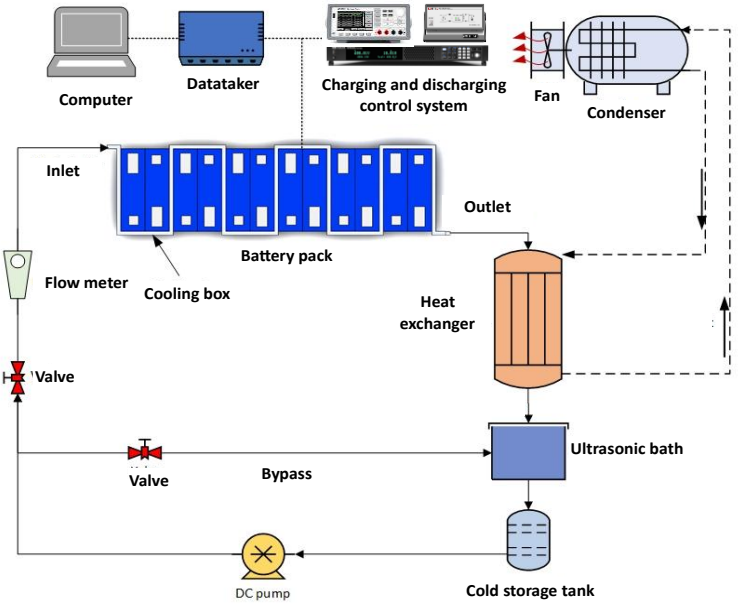

Fig. 5: Schematic diagram of the experimental apparatus.

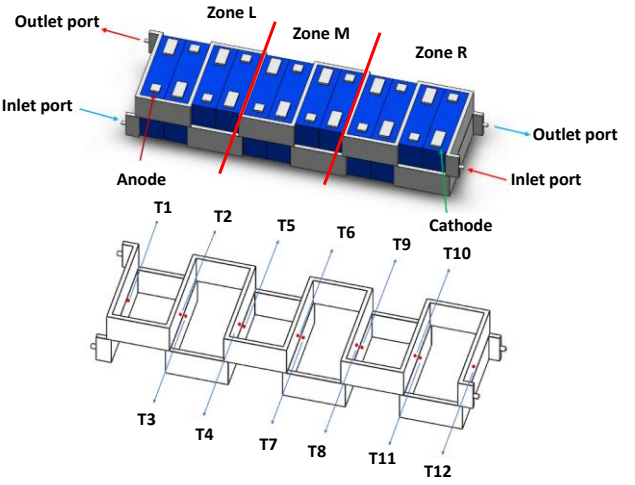

Fig. 6: Details of thermocouple installation.

$$\mu_{nf} = (1 + 2.5\phi)\mu_w \quad (1)$$

$$k_{nf} = \left[\frac{k_p + 2k_w - 2\varphi(k_w - k_p)}{k_p + 2k_w + \varphi(k_w - k_p)}\right] k_w \quad (2)$$

$$\rho_{nf} = \phi\rho_P + (1 - \phi)\rho_w \quad (3)$$

$$(\rho C_p)_{nf} = \phi(\rho C_p)_p + (1 - \phi)(\rho C_p)_w \quad (4)$$

where φ is the ferroparticles volume fraction, k_{nf} is the ferrofluid thermal conductivity, k_w is the base fluid's thermal conductivity, k_p is the ferroparticles thermal conductivity $(\rho C_p)_{nf}$ is the ferrofluid heat capacity, $(\rho C_p)_w$ is the base fluid heat capacity, $(\rho C_p)_p$ is the ferroparticles heat capacity, ρ_{nf} is the ferrofluid density, ρ_p is the ferroparticles density, ρ_w is the base fluid density, μ_{nf} is the ferrofluid viscosity, and μ_w is the base fluid viscosity.

2.3 The battery pack

The liquid cooling systems potential dangers to user safety should be the top priority. In this investigation, the cold fluid enters the battery pack via the cooling jacket's indirect-contact heat transfer route. The cooling jacket of the battery pack is made of an aluminum block. Before the battery cells are installed, each portion of the jacket is joined using welding and tested for leakage. Li-ion batteries are becoming more popular for various uses, including but not limited to electric cars and portable gadgets. This study solely employs analysis of the 12 lithium-ion battery cells. The electric vehicle's battery pack, shown in Fig. 7, comprises the battery pack and two layers of a liquid cooling package. At the top layer zone, the coolant flows into the liquid cooling package; at the other end, it flows out. In the second, similar to a counter-current flow, the coolant enters the zone at the bottom and exits at the opposite end. Please ensure all battery cells are at least 75% full before testing the battery pack. You can find all the information about the battery cells in Table 2. To get 38.4V and 50A, the electrical battery pack's 12 cells are linked in series. A BMS device regulates the current and voltage that goes into the battery. Fig. 5 shows the power supply and the appropriate equipment to illustrate the charged and discharged operations.

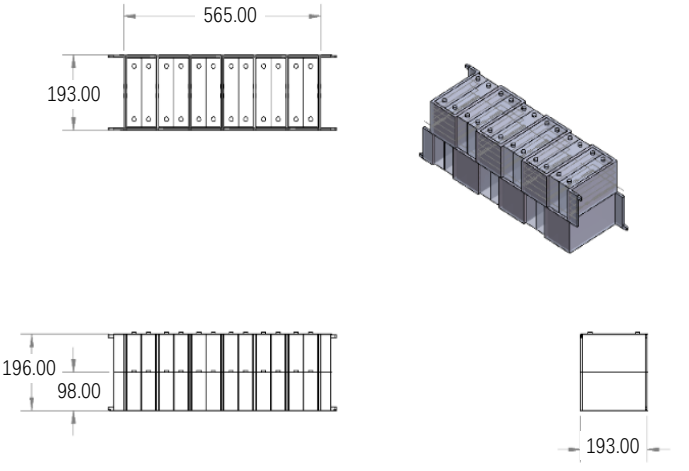

Fig. 7: Dimensions of the battery cooling module.

Table 2: Details of the prismatic $LiFePO_4$ battery.

Properties	Specification
Electrolyte material chemistry	Lithium Iron Phosphate
Dimension (Width*Length*High)	42*177*98 mm
Weight	1395 g
Nominal capacity	50 Ah
Nominal voltage	3.2 V
Charge cut-off voltage	3.65V (100% SOC)
Discharge cut-off voltage	2.50V (0% SOC)
Number of cells	12
Total voltage	38.4 V

Table 3: Uncertainty and accuracy of the instruments.

Instruments	Accuracy	Uncertainty
Voltage supplied by power source, voltage	0.20%	±0.50
Current supplied by power source, ampere	0.20%	±0.50
Digital weight scale, gram	0.01%	±0.01
Thermocouple type T, Data logger, ^oC	0.10%	±0.10
Differential pressure transducer	0.02%	±0.02

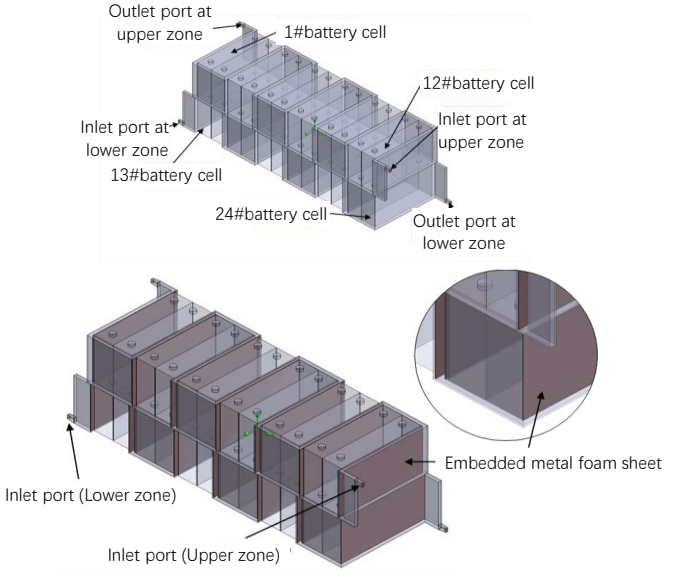

Fig. 8: Details of the computational domain with porous media sheet.

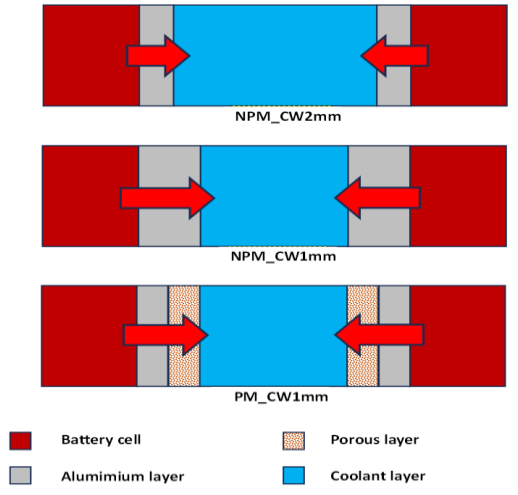

Fig. 9: Details of the three different flow channels with and without porous media sheet.

2.4 Experimental procedure

The uncertainty and accuracy of the relevant instruments are shown in Table 3. To investigate the transient thermal response of the battery unit over time, the charging and discharging procedures are carried out without the circulation of liquid cooling at 0.8A-1A at varying current rates. The total temperature of the module is significantly affected by the discharge/charge current rates. Avoid utilizing a very high charge/discharge current. Although the battery temperature is hard to monitor, the cell is full and drains rapidly. Thus, 0.8A-1A current rates are used for charging and discharging. The standard calibrator calibrates the voltage and current with errors of ±0.5V and ±0.05A, respectively, since the pack is linked to the power source and controlled by the BMS. The first flow enters at the top of the cooling jacket, while the second current exits at the bottom.

3. Mathematical modeling

3.1 The main equations

Fig. 8 shows flow diagrams of the computational domain with and without copper foam sheets. Battery cooling jackets are used in mathematical models based on ferrofluid. Three models with different flow channel widths and with/without copper foam sheets have been analyzed, as shown in Fig. 9. The Eulerian two-phase flow model is founded on principles such as homogeneity of the mixture, constant flow, the absence of phase change, and viscous dissipation.[73,74] Continuity equations of each phase are in Eq.(5). Momentum equations are given in Eqs. (6) and (7).

$$\nabla(\rho_p\phi_p V_p) = 0,\ \nabla(\rho_l\phi_l V_l) = 0 \tag{5}$$

$$\nabla(\rho_p\phi_p V_p V_p) = \phi_p\nabla P + \nabla\left(\phi_p\mu_p\left(\nabla V_p + \nabla V_p T\right)\right) - F_d + F_{Vm} + F_{cd} \tag{6}$$

$$\nabla(\rho_l\phi_l V_l V_l) = \phi_l\nabla P + \nabla\left(\phi_l\mu_l(\nabla V_l + \nabla V_l T)\right) + F_d + F_{Vm} \tag{7}$$

The following methods exist for characterizing the drag force between nanoparticles floating in water,[75] as in Eqs. (8)-(13).

$$F_d = -\beta\left(V_l - V_p\right) \tag{8}$$

$$\beta = C_d\frac{3(1-\phi_l)\phi_l}{4d_p}\left(V_l - V_p\right)\phi_l^{-265} \tag{9}$$

$$C_d = \begin{cases}\frac{24}{Re_p}\left(1 + 0.15Re_p^{0.687}\right), & Re_p\langle 1000\\ 0.44\,, & Re_p\rangle 1000\end{cases} \tag{10}$$

$$Re_p = \frac{\phi_l|V_l - V_p|d_p}{\nu_l} \tag{11}$$

The virtual mass force grows in direct proportion to the relative acceleration, as stated in Ref. [76].

$$F_{vm} = \frac{0.5\phi_p\rho_l D(V_l - V_p)}{Dt} \tag{12}$$

The proposed correlation defines mutual contact force and modulus.[77]

$$F_{cd} = \phi_l\vec{\nabla}\phi_l\{exp(-600[\phi_l - 0.376])\} \tag{13}$$

Energy equations are shown below. We may rewrite the energy equation by considering the nanofluids' two phases as in Eqs. (14) and (15).

$$\nabla\left(\rho_l\phi_l C_{p,l}T_l V_l\right) = \nabla(\phi_l k_l\nabla T_l) - h_v\left(T_l - T_p\right) \tag{14}$$

$$\nabla\left(\rho_p\phi_p C_{p,p}T_p V_p\right) = \nabla\left(\phi_p k_p\nabla T_p\right) - h_v\left(T_l - T_p\right) \tag{15}$$

Here are the many shapes that the mono-dispersed particles (hv), as in Eq. (16), may take:

$$h_v = \frac{6(1-\phi_l)h_p}{d_p} \tag{16}$$

Here is the heat transfer coefficient between fluid particles, as given in Eq. (17).[78]

$$h_p = \left(2 + 1.1Re_p^{0.6}Pr^{1/3}\right)\frac{k_l}{d_p} \tag{17}$$

What follows is a proposal for the effective thermal conductivities of liquids and particles (k_l, k_p) made by Ref. [79], as in Eqs. (18)-(22).

$$k_p = \frac{k_{bp}}{\phi_p},\ k_l = \frac{k_{bl}}{\phi_l} \tag{18}$$

$$k_{bp} = \left(\sqrt{(1-\phi_l)}\right)\left(7.26\times10^{-3}\frac{k_p}{k_l} + 0.9927\Gamma\right)k_l \tag{19}$$

$$k_{bl} = \left(1 - \sqrt{(1-\phi_l)}\right)k_l \tag{20}$$

$$\Gamma = \frac{2A}{(A-B)}\left\{\frac{AB(A-1)}{(A-B)^2}\right\} ln\left(\frac{A}{B}\right) - \frac{(AB-A)}{(A-B)} - \frac{B+1}{2} \quad (21)$$

$$A = \frac{k_p}{k_l}, B = 1.25\left(\frac{1}{\phi_l} - 1\right)^{\frac{10}{9}} \quad (22)$$

Table 4: Initial parameters used in the numerical analysis.

Parameters	Units	Values
Room temperature	°C	30
Inlet coolant velocity (Upper and lower zones)	m/s	0.2
Metal foam porosity	-	0.50, 0.70, 0.98
Metal foam pore size	mm	0.25
Specific heat capacity of metal foam	J/(kg*K)	390
Thermal conductivity of metal foam	W/(m*K)	1000
Inlet coolant temperature	°C	25
Generated heat from the battery pack	W/m^3	174

3.2 Boundary conditions

The design of the fluid flow channel may be improved to more effectively imitate battery conditions by including two separate layers of coolant flow directions. Insulation was attached to the battery top and bottom and the channel outside to prevent heat loss. Furthermore, to guarantee effective heat transfer throughout the system, the coolant-to-cell surface walls were coupled, the intake velocities were set to mimic boundary conditions, and the cooling fluids were selected to mimic those used in the packs closely. Including all required components, such as insulation and boundary conditions, is the final stage in constructing an accurate pack model. Characteristics of the nanofluid include Newtonianity and incompressibility. The initial relevant parameters are shown in Table 4. The boundary conditions are presented as follows.

Inlet port: The inlet of coolant temperature and inlet velocity are set as $T = T_{in}, V = V_{in}$;

Outlet port: The outlet of coolant pressure is set as $P_{out} = o$;

Battery cell wall: The heat rate from battery cells is generated as $q = q_{in}$;

The outside surface of the cooling pack: adiabatic;

The battery cell and the aluminum interface: $-k_{ba}\frac{\partial T}{\partial n} = -k_{al}\frac{\partial T}{\partial n}$.

3.3 Computational methodology and grid-independent test

The outcomes of the numerical analysis using three distinct models are shown in Fig. 9. Researchers used the MSMD approach in FLUENT Software to simulate a battery pack's electrical and thermal characteristics. Many real-world engineering applications exist for the ANSYS program. After creating the model and mesh, the ANSYS Fluent program takes a SIMPLE approach—which incorporates velocity and pressure—to solve the problems related to the required boundary conditions. It simplifies the pressure-velocity calculations and makes complex fluid flow problems easier to solve. It is critical to establish appropriate convergence criteria to get reliable simulation results. Our analysis used the RMS residual level convergence criterion of 10^{-6} to ensure the simulation results were within acceptable limits. A high-powered system with demanding computational requirements might have 18 CPU cores and 96 GB of RAM.

Because it ensures the results are precise and dependable, the mesh independence test method is the most essential component of the procedure. You may tweak the mesh grid and get more precise results by using three unique mesh numbers to determine when it stops making a significant impact. In Fig. 10, we can see the grid arrangement. Choosing the lowest possible mesh size simplifies the simulation execution, lowering computational effort and overall runtime. Using a coolant velocity of 0.02 m/s on the cooling jacket, we applied 25 °C inlet temperatures into the cooling channel. We averaged the pack temperatures over grid numbers to examine the effect on the forecasts. Using the mesh independence approach, we observed that temperature measurements from various grid numbers differed little. Since the predicted results were independent of the grid numbers, as shown in Fig. 11, we can say that the method was stable and valid. Grid numbers of 1,521,000 were used for the subsequent simulations to accurately reflect the battery fluid flow and heat transfer while maximizing processing efficiency. Despite a strong relationship between temperature and variance, the coarse and medium meshes differ most. Nevertheless, the mesh resolution is enough as this is below the 1% tolerance for computational fluid dynamics (CFD) solutions.

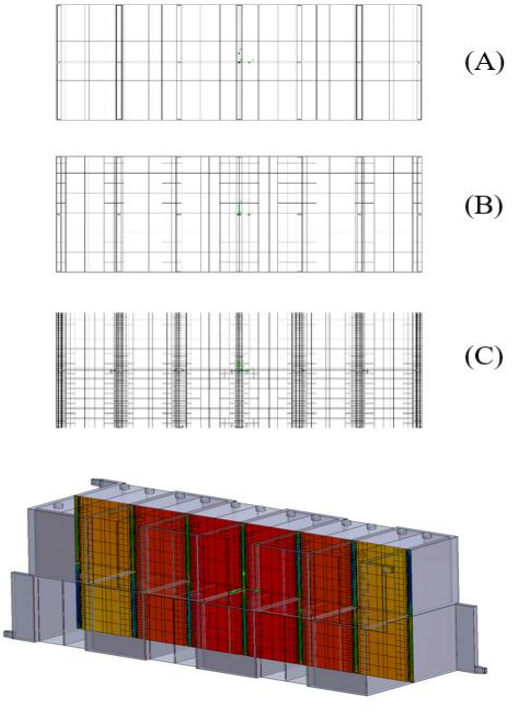

Fig. 10: Grid characteristics used in the present numerical analysis.

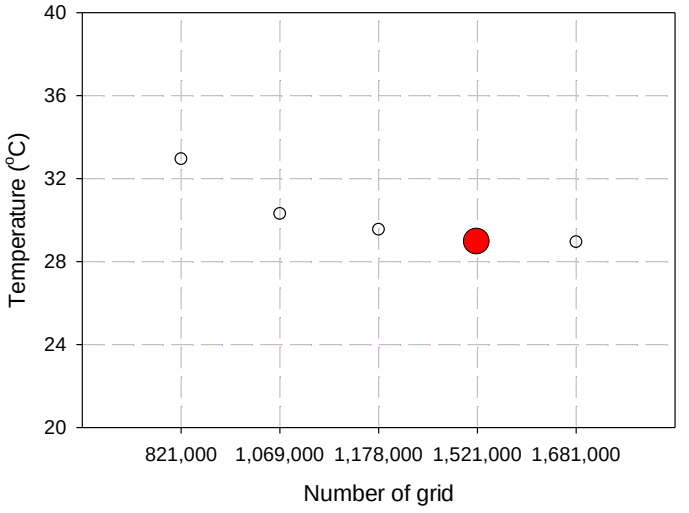

Fig. 11: Grid characteristics used in the present numerical analysis.

4. Results and discussion

The effects of the surrounding air temperature were reduced by keeping the experimental settings at a constant 25-27 °C. It was necessary to perform the experimental operations at a low C-rate due to the limitations imposed by the charging and discharging control system. Energy storage battery charging took 30 minutes, and discharging it took 30 minutes, as shown in the system pre-test. Keep the temperature below 40 °C to keep the pack stable and secure and extend its lifetime.[80] Verifying the numerical study data is necessary to confirm the anticipated results. We prepared the experimental set and developed cooling models to verify our expectations. To confirm the projected outcomes, we used the mean battery pack temperatures from each zone (Zone L, Zone M, and Zone R) for the model. Table 5 shows that the model has a zone L error of 5.79%, zone M error of 4.95%, and zone R error of 5.51%.

Table 5: Comparison of the outlet coolant and average battery temperature from the measured data and the present predicted results without the metal foam sheet.

Parameters	Results		
	Measured data	Predicted results	% Errors
Average battery temperature at zone L	32.54	30.71	5.79
Average battery temperature at zone M	33.73	32.10	4.95
Average battery temperature at zone R	32.23	30.5	5.51

In the experiment, the coolant entering the pack is divided into two paths: in the first path, the coolant flows into the pack from the left-hand side at the lower zone. Then, it flows out the battery pack at the opposite side on the right-hand side. In the second path, the coolant flows into the pack from the right side of the upper zone and flows out from the opposite side on the left-hand side. Both flow characteristics are in the counter-current flow. The temperature variations of the cells in the module are measured at 12 points, as shown in Fig. 6. Fig. 12 shows the temperature variation of the pack with a single cycle (charged and discharged processes). All temperatures are measured at the middle point between the upper and lower channels, in which two coolant streams are in the counterflow arrangement. The generated heat is more than the removal of heat capacity. In the charged and discharged processes, the battery cell temperature significantly tends to increase with operating time (with cooling case). Therefore, the central zone's battery pack temperature is the highest due to heat accumulation during the charging and discharged processes. Therefore, the temperatures at the middle zone (T6, T7) are higher than those at the two ends (T2, T3), (T10, T11) of the cooling pack. In addition, the temperature variation characteristics from the experiment were similar to the experimental results of previous research in which the charging and discharging processes include small dips and little climbs.[3] The temperature fluctuations that occur throughout these operations are likewise rather constant. Discharging causes a greater temperature rise than charging due to the lower response in the former. When inserted and removed between two poles, lithium ions generate heat during the process. The processes that include charges undergo an endothermic reaction, whereas those that involve discharges undergo an exothermic reaction. On the whole, there are two ways in which batteries may produce heat: reversible and irreversible. Overpotential and electrical resistances generate the irreversible mode, whereas entropy change within the battery produces the reversible heat mode. In their proposal for an Eq.(23) to represent the battery's heat generation, Bernardi *et al*.[81] state:

$$Q = \pm I(U_{ca} - U_{an} - U) - I\left(T\frac{d(U_{ca}-U_{an})}{dT}\right) \quad (23)$$

The irreversible heat mode is denoted as $I(U_{ca}\text{-}U_{an}\text{-}U)$, where I is the current, U_{ca} and U_{an} are the cathode and anode poles of the open circuit potential (OCP), U is the terminal voltage, and T is the temperature. In the second term, we have the entropy change, which causes the reversible heat to change. The entropy coefficient, defined as the differential of U_{ca} and U_{an} divided by dT, depends on the energy density, the state of charge (SOC), and temperature. Reversible heat is predominant at low current rates, but irreversible heat dominates at high current rates.[82] With an increase in either the current rate or the nominal battery capacity, as well as an increase in both the charging and discharging processes, the irreversible heat rises.[80]

Because of space constraints, only typical findings are given; however, many graphs may be made from the study's data. Fig. 13 shows sampled model cross-sections used for data display. Fig. 14 shows the variation of battery cell temperatures for the XZ plane (A) y = 0 mm, (B) y = 40 mm, (C) y = 80 mm obtained from different models. The none-

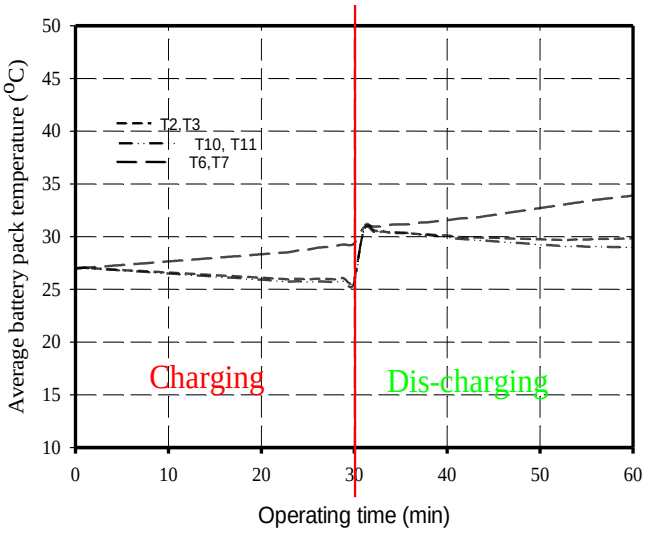

Fig. 12: Variation of battery cell temperature with operating time.

porous media with channel width = 2 mm (NPM_CW2mm) represents the battery cooling pack with a channel width of 2 mm without copper foam, the NPM_CW1mm represents the battery cooling pack with a channel width of 1 mm without copper foam, and the PM_CW1mm represents the battery cooling pack with a channel width of 1 mm with copper foam. The cross-sections of y=0 and y=80 mm locate the middle and upper layers of the battery pack, respectively. Two coolant paths enter the battery pack at the top and bottom layers as the counter-current flow, which results in the hottest temperature occurring at the middle layer. In contrast, the coldest temperature occurs at the middle layer due to the closed inlet coolant port. Without the copper foam at the same layer, it can be seen that the temperatures of the model NPM_CW1mm are lower than those from the NPM_CW2mm. This is because the removal ability of the coolant depends on the maximum velocity flowing in the cooling flow channel.

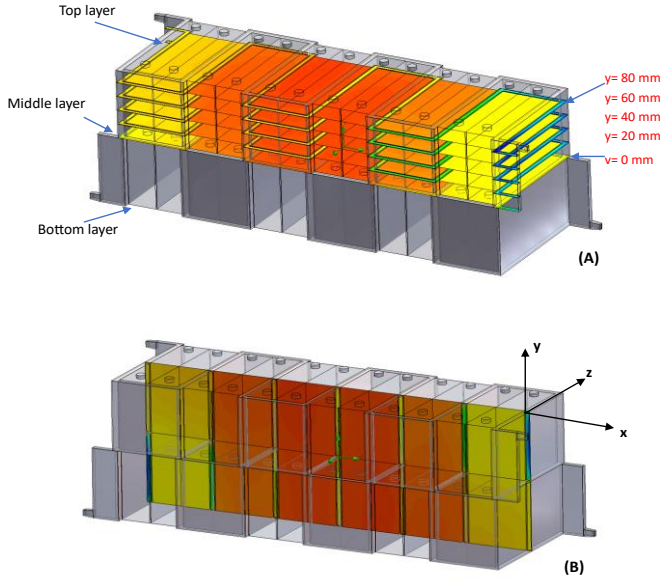

Fig. 13: Cross-section layer for obseving the temperature distribution (A) XZ plane and (B) XY plane.

Fig. 14 also shows the effect of copper foam on the cooling ability of the pack. The copper foam sheet with a porosity of 0.98 is embedded on the flow channel's inside surface. The PM_CM1mm gives the battery pack temperature less than two models without copper foam. As shown in Fig. 9, the heat transfer from the cell to the aluminum layer by conduction mode and then to the copper foam layer by conduction and convection modes. Nanofluids with porous copper foam improve heat transmission by the following method. Adding nanoparticles to a base fluid may boost its effective thermal conductivity, and the energy transfer between the two is amplified by the nanoparticles' Brownian motion and the influence of their tiny size. In contrast, the metallic properties and intricate three-dimensional porosity of porous copper foam set it apart. Not only does it allow for robust transverse mixing, but it also has a big heat transmission area and capillary force, which results in higher turbulent mixing tensity of coolant near the contact surface zone, resulting in higher heat removal ability. Therefore, the battery cell temperatures for the cooling model embedded with the copper foam sheet are lower than those without the copper foam sheet, as shown in Fig. 14. For XY plane at z=0 mm, the minimum battery cell temperature occurs at both sides and tends to the maximum point at the central zone of the pack, as shown in Fig. 15. At the same layer, the hottest cell temperature occurs at the central area of the pack and then tends to decrease on both sides, as shown in Fig. 16. For the whole length of the flowing channel, the highest battery cell temperature is from the NPM_CW2mm, the NPM_CW1mm, and the PM_1mm, respectively.

Fig. 17 shows the variation of each cell obtained from three different cooling models. From three different cooling models, the hottest and coldest zones occur at the central and both sides of the pack, respectively. For the model NPM_CW2mm, the maximum and the minimum temperatures are 32 ºC and 30 ºC, respectively. The model NPM_CW1mm gives the maximum and minimum temperatures of 30.2 ºC and 28.6 ºC, respectively. The maximum battery cell for the cooling model with copper foam sheet is 29.4 ºC, and 28.2 ºC for the minimum temperature.

Fig. 18 shows the effect of copper foam's porosity on the pack's cooling performance. The coolant's temperature difference is the outlet temperature minus the inlet temperature. Copper foam significantly affects cooling performance and gives the difference values of 4.3 ºC without copper foam sheets. The heat transfer enhancement for a porosity of 0.5, 0.7, and 0.98 are 11.89%, 11.19%, and 11.20%, respectively. Higher porosity results in higher heat transfer surface area. Nevertheless, the cooling model with the copper foam layer results in a larger pressure drop throughout the cooling channel compared to one without the sheet, mostly because of the irregular pore shape. Fig. 19 shows that it then tends to rise as the porosity of the copper foam increases. There is a pressurized drop increment of 23.11% for 0.5, 24.32% for 0.7, and 24.82% for 0.98. The resistance to flow

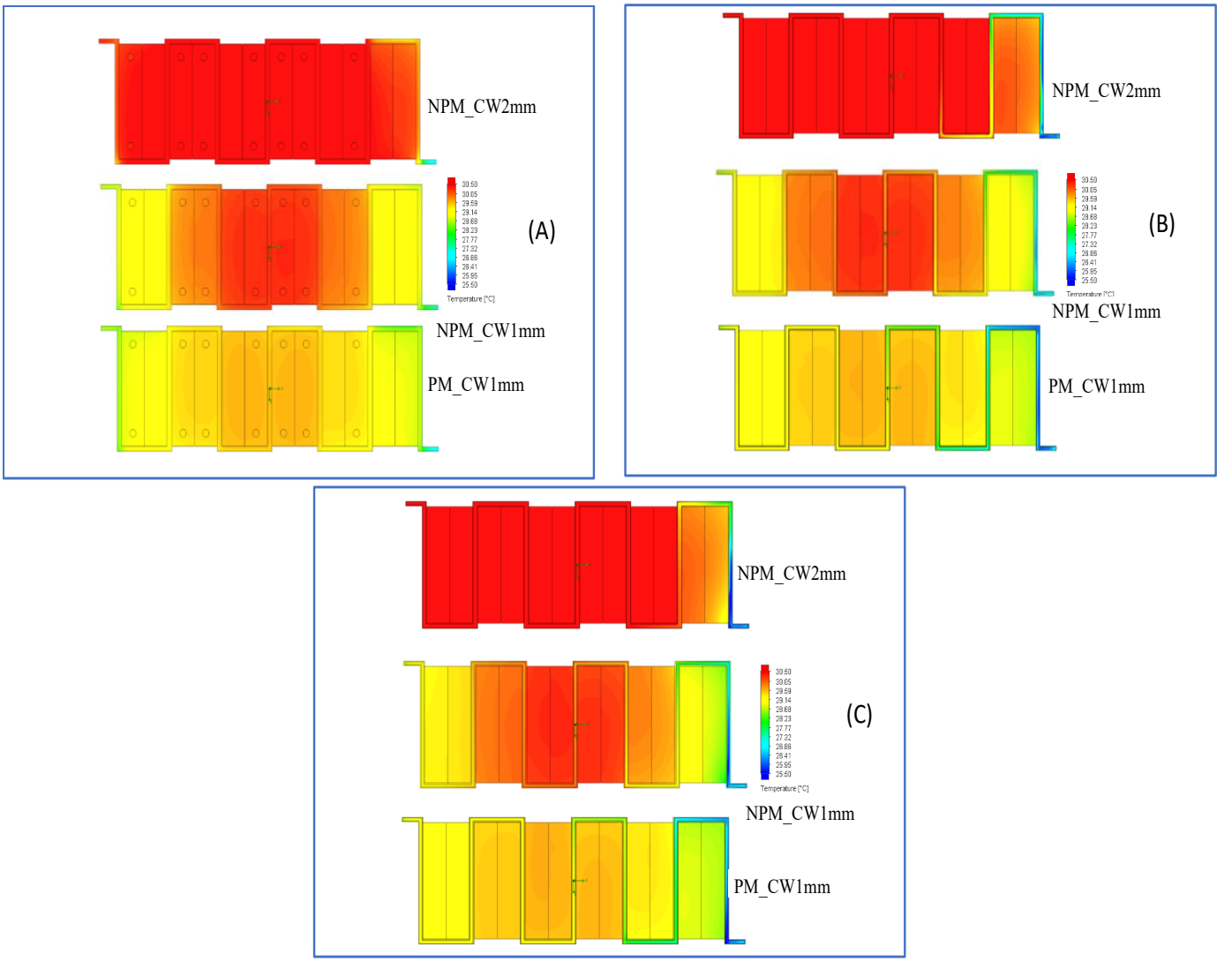

Fig. 14: Variation of temperatures for XZ plane (A) y = 0 mm, (B) y = 40 mm, and (C) y = 80 mm.

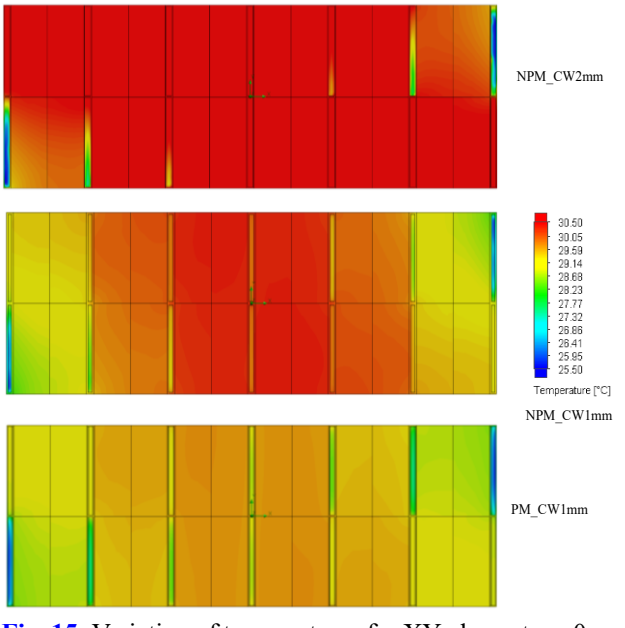

Fig. 15: Variation of temperatures for XY plane at z = 0 mm.

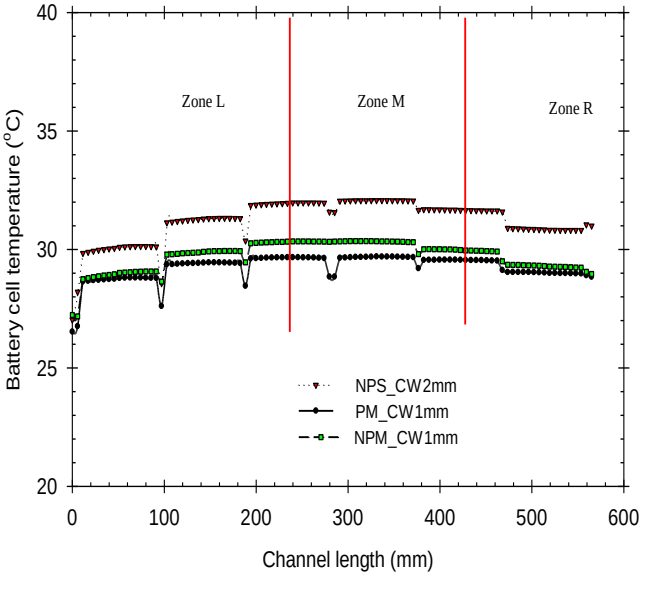

Fig. 16: Variation of temperatures with channel length at y = 40 mm.

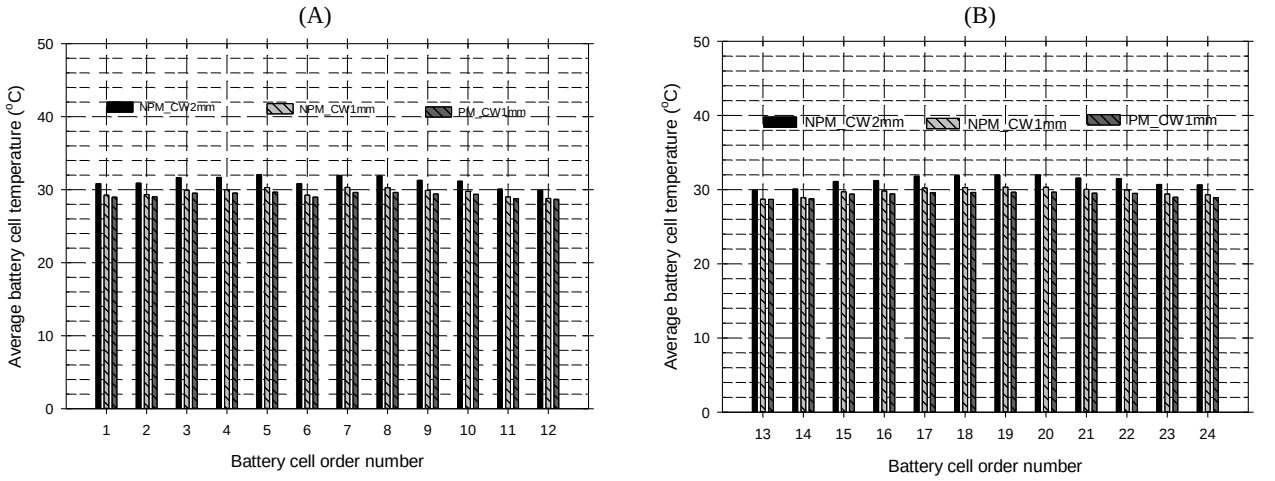

Fig. 17: Variation of average battery cell temperatures of each model for (A) the 1st -12th cell and (B) the 13th -24th cell.

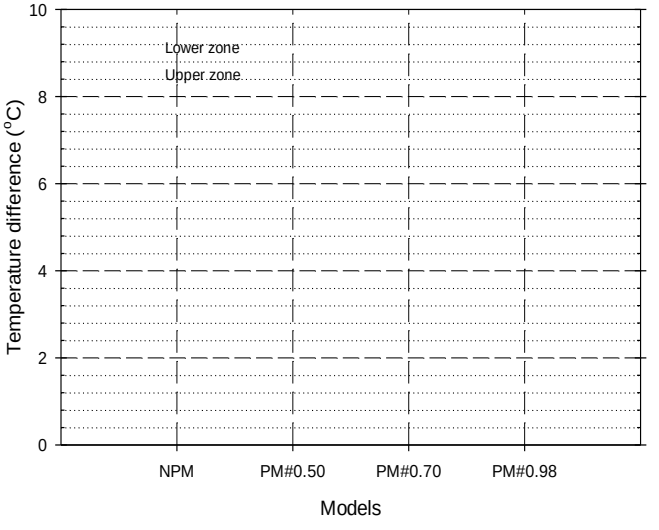

Fig. 18: Effect of porosity of copper foam on coolant temperature difference.

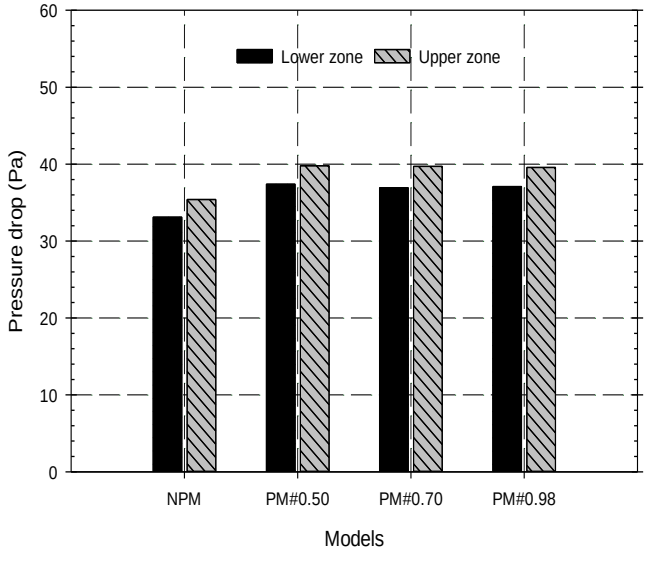

Fig. 19: Effect of porosity of copper foam on pressure drop in the flow channel.

increases as the channel gets more turbulent. A higher porosity of copper foam results in a greater inertial drag due to separation flow inside the structure. All of these things contribute to a greater pressure drop inside the flow channel. For the reasons already stated, a sensitivity analysis is run on the convective heat transfer within a porous heat exchanger to determine how different porous materials affect the rate of heat transfer and the pressure drop. In this case, the porosity of the copper foam significantly impacts the latter more than the former.

Due to the correlation between improved heat transfer and lower pumping costs, improving heat transfer and reducing pressure drop are two of the most critical goals in the design of heat transfer devices. Heat transfer enhancement is positively affected by porous materials, whereas pressure drop is negatively affected. These findings may serve as a starting point for data collection on the many parameters to be employed in the manufacturing of heat exchangers, and they also provide helpful recommendations for their design. Both the improvement of heat transmission and the reduction of pressure drop are affected by a number of important specifications. Experimentation should, therefore, be carried out, taking into account the impact of the most relevant factors.

5. Conclusion

For optimal temperature control in packs and complete protection against overheating, a coolant medium must be used to transfer heat to the cooling system. The ideal qualities of a coolant medium are low cost, non-toxicity, sizeable thermal capacity, and low viscosity; a coolant is a kind of heat transfer cooling medium. In this research, we used nanofluid to boost the thermal cooling of an electric vehicle's battery pack by passing it down a conduit filled with copper foam sheets. When comparing the three versions, it is clear that the one with the copper foam layer for cooling produces a cooler battery pack. The resistance to flow increases as the channel gets more turbulent. A higher porosity of copper foam results in a larger surface area for heat transmission and increased

inertial drag due to separation flow inside the structure. Because of these considerations, the pressure drop and heat removal capabilities inside the flow channel are both improved. Designing heat transfer devices with increased heat transfer and reduced pressure drop as the primary aim is essential because of the association between the two and reduced pumping costs. With these results in hand, researchers may begin to compile a list of all the variables that will go into making heat exchangers, and designers will have a better idea of how to proceed. Improving heat transfer and reducing pressure loss are both impacted by many critical criteria. Therefore, when conducting experiments, it is important to consider the influence of the most important components.

Acknowledgments
Srinakharinwirot University's (SWU) Faculty of Engineering generously supported this research, and the authors are grateful to them.

Conflict of Interest
There is no conflict of interest.

Supporting Information
Not applicable.

Nomenclatures

A	defined in Eq. (22), [-]
B	defined in Eq. (22), [-]
BTMS	battery thermal management system
C_d	defined in Eq. (10), [-]
C_p	specific heat, [kJ kg^{-1} ^{o}C^{-1}]
d	diameter, [m]
EV	electric vehicle
F	force, [N]
h	heat transfer coefficient, [kW m^{-2} ^{o}C^{-1}]
h_p	fluid-particle heat transfer coefficient, [kW m^{-2} ^{o}C^{-1}]
h_v	volumetric interphase heat transfer coefficient, [kW m^{-3} ^{o}C^{-1}]
I	current, [ampere]
k	thermal conductivity, [kW m^{-1} ^{o}C^{-1}]
k_{bl}	defined in Eq. (20), [kW m^{-1} ^{o}C^{-1}]
k_{bp}	defined in Eq. (19), [kW m^{-1} ^{o}C^{-1}]
Li-ion	Lithium-ion
NPM	none porous media
OCP	open circuit potential
P	pressure, [kPa]
PCM	phase change material
PM	porous media
q	heat flux [kW m^{-2}]
Re	Reynolds number
SOC	state of charge
T	temperature, [^{o}C]
U	potential [voltage]
V	velocity, [m s^{-1}]

Greek symbols

ϕ	nanofluid concentration, [%]
ρ	density, [kg m^{-3}]
β	defined in Eq. (9), [kg m^{-3}s^{-1}]
μ	viscosity, [kg m^{-1}s^{-1}]
Γ	defined in Eq. (21), [-]

Subscripts

al	alumimium
an	anode
ba	battery cell
ca	cathode
cd	drag coefficient
d	drag force
in	inlet
l	liquid
p	particles
Vm	virtual mass
out	outlet

References

[1] K. J. Kelly, M. Mihalic, M. Zolot, Battery usage and thermal performance of the Toyota Prius and Honda Insight during chassis dynamometer testing, Seventeenth Annual Battery Conference on Applications and Advances, Proceedings of Conference, January 18, 2002, Long Beach, CA, USA. IEEE, 2002, 247-252, doi: 10.1109/BCAA.2002.986408.

[2] Q. Wang, B. Jiang, B. Li, Y. Yan, A critical review of thermal management models and solutions of lithium-ion batteries for the development of pure electric vehicles, *Renewable and Sustainable Energy Reviews*, 2016, **64**, 106-128, doi: 10.1016/j.rser.2016.05.033.

[3] A. A. Pesaran, Battery thermal models for hybrid vehicle simulations, *Journal of Power Sources*, 2002, **110**, 377-382, doi: 10.1016/S0378-7753(02)00200-8.

[4] G. Zhao, X. Wang, M. Negnevitsky, H. Zhang, A review of air-cooling battery thermal management systems for electric and hybrid electric vehicles, *Journal of Power Sources*, 2021, **501**, 230001, doi: 10.1016/j.jpowsour.2021.230001.

[5] H. Liu, Z. Wei, W. He, J. Zhao, Thermal issues about Li-ion batteries and recent progress in battery thermal management systems: A review, *Energy Conversion and Management*, 2017, **150**, 304-330, doi: 10.1016/j.enconman.2017.08.016.

[6] P. Kumar, D. Chaudhary, P. Varshney, U. Varshney, S. M. Yahya, Y. Rafat, Critical review on battery thermal management and role of nanomaterial in heat transfer enhancement for electrical vehicle application, *Journal of Energy Storage*, 2020, **32**, 102003, doi: 10.1016/j.est.2020.102003.

[7] W. Li, M. Xiao, X. Peng, A. Garg, L. Gao, A surrogate thermal modeling and parametric optimization of battery pack with air cooling for EVs, *Applied Thermal Engineering*, 2019, **147**, 90-100, doi: 10.1016/j.applthermaleng.2018.10.060.

[8] N. Yang, X. Zhang, G. Li, D. Hua, Assessment of the forced air-cooling performance for cylindrical lithium-ion battery packs: A comparative analysis between aligned and staggered cell arrangements, *Applied Thermal Engineering*, 2015, **80**, 55-65,

doi: 10.1016/j.applthermaleng.2015.01.049.
[9] L. H. Saw, Y. Ye, A. A. O. Tay, W. T. Chong, S. H. Kuan, M. C. Yew, Computational fluid dynamic and thermal analysis of Lithium-ion battery pack with air cooling, *Applied Energy*, 2016, **177**, 783-792, doi: 10.1016/j.apenergy.2016.05.122.
[10] K. Chen, W. Wu, F. Yuan, L. Chen, S. Wang, Cooling efficiency improvement of air-cooled battery thermal management system through designing the flow pattern, *Energy*, 2019, **167**, 781-790, doi: 10.1016/j.energy.2018.11.011.
[11] T. Wang, K. J. Tseng, J. Zhao, Development of efficient air-cooling strategies for lithium-ion battery module based on empirical heat source model, *Applied Thermal Engineering*, 2015, **90**, 521-529, doi: 10.1016/j.applthermaleng.2015.07.033.
[12] E. Jiaqiang, M. Yue, J. Chen, H. Zhu, Y. Deng, Y. Zhu, F. Zhang, M. Wen, B. Zhang, S. Kang, Effects of the different air cooling strategies on cooling performance of a lithium-ion battery module with baffle, *Applied Thermal Engineering*, 2018, **144**, 231-241, doi: 10.1016/j.applthermaleng.2018.08.064.
[13] K. A. M. Alharbi, G. F. Smaisim, S. M. Sajadi, M. A. Fagiry, H. S. Aybar, S. E. Elkhatib, RETRACTED: Numerical study of lozenge, triangular and rectangular arrangements of lithium-ion batteries in their thermal management in a cooled-air cooling system, *Journal of Energy Storage*, 2022, **52**, 104786, doi: 10.1016/j.est.2022.104786.
[14] K. Chen, M. Song, W. Wei, S. Wang, Structure optimization of parallel air-cooled battery thermal management system with U-type flow for cooling efficiency improvement, *Energy*, 2018, **145**, 603-613, doi: 10.1016/j.energy.2017.12.110.
[15] Y. Liu, J. Zhang, Design a J-type air-based battery thermal management system through surrogate-based optimization, *Applied Energy*, 2019, **252**, 113426, doi: 10.1016/j.apenergy.2019.113426.
[16] X. Lin, K. Shao, C. Wang, Optimization and numerical simulation of novel air-cooling system for the thermal management of lithium-ion battery pack, *International Journal of Electrochemical Science*, 2022, **17**, 220141, doi: 10.20964/2022.01.12.
[17] X. Lan, X. Li, S. Ji, C. Gao, Z. He, Design and optimization of a novel reverse layered air-cooling battery management system using U and Z type flow patterns, *International Journal of Energy Research*, 2022, **46**, 14206-14226, doi: 10.1002/er.8136.
[18] D. Kang, P.-Y. Lee, K. Yoo, J. Kim, Internal thermal network model-based inner temperature distribution of high-power lithium-ion battery packs with different shapes for thermal management, *Journal of Energy Storage*, 2020, **27**, 101017, doi: 10.1016/j.est.2019.101017.
[19] T. M. Bandhauer, S. Garimella, T. F. Fuller, A critical review of thermal issues in lithium-ion batteries, *Journal of the Electrochemical Society*, 2011, **158**, R1, doi: 10.1149/1.3515880.
[20] S. Panchal, I. Dincer, M. Agelin-Chaab, R. Fraser, M. Fowler, Thermal modeling and validation of temperature distributions in a prismatic lithium-ion battery at different discharge rates and varying boundary conditions, *Applied Thermal Engineering*, 2016, **96**, 190-199, doi: 10.1016/j.applthermaleng.2015.11.019.
[21] D. Chen, J. Jiang, G.-H. Kim, C. Yang, A. Pesaran, Comparison of different cooling methods for lithium-ion battery cells, *Applied Thermal Engineering*, 2016, **94**, 846-854, doi: 10.1016/j.applthermaleng.2015.10.015.
[22] P. Li, J. Liu, Self-driven electronic cooling based on thermosyphon effect of room temperature liquid metal, *Journal of Electronic Packaging*, 2011, **133**, 041009, doi: 10.1115/1.4005297.
[23] M. Liu, M. C. Lin, C. Y. Tsai, C. Wang, Enhancement of thermal conductivity with Cu for nanofluids using chemical reduction method, *International Journal of Heat and Mass Transfer*, 2006, **49**, 3028-3033, doi: 10.1016/j.ijheatmasstransfer.2006.02.012.
[24] O. Kalaf, D. Solyali, M. Asmael, Q. Zeeshan, B. Safaei, A. Askir, Experimental and simulation study of liquid coolant battery thermal management system for electric vehicles: A review, *International Journal of Energy Research*, 2021, **45**, 6495-6517, doi: 10.1002/er.6268.
[25] Y. Deng, C. Feng, E. Jiaqiang, H. Zhu, J. Chen, M. Wen, H. Yin, Effects of different coolants and cooling strategies on the cooling performance of the power lithium ion battery system: A review, *Applied Thermal Engineering*, 2018, **142**, 10-29, doi: 10.1016/j.applthermaleng.2018.06.043.
[26] P. Nelson, D. Dees, K. Amine, G. Henriksen, Modeling thermal management of lithium-ion PNGV batteries, *Journal of Power Sources*, 2002, **110**, 349-356, doi: 10.1016/S0378-7753(02)00197-0.
[27] Y. Yang, W. Li, X. Xu, G. Tong, Heat dissipation analysis of different flow path for parallel liquid cooling battery thermal management system, *International Journal of Energy Research*, 2020, **44**, 5165-5176, doi: 10.1002/er.5089.
[28] C. Wang, G. Zhang, X. Li, J. Huang, Z. Wang, Y. Lv, Experimental examination of large capacity liFePO4 battery pack at high temperature and rapid discharge using novel liquid cooling strategy, *International Journal of Energy Research*, 2018, **42**, 1172-1182, doi: 10.1002/ER.3916.
[29] Z. Guo, S. Zhao, J. Wang, Y. Wang, S. Zhai, T. Zhao, M. Ni, Novel battery thermal management system with different shapes of pin fins, *International Journal of Energy Research*, 2022, **46**, 5997-6011, doi: 10.1002/er.7539.
[30] S. Wiriyasart, C. Hommalee, S. Sirikasemsuk, R. Prurapark, P. Naphon, Thermal management system with nanofluids for electric vehicle battery cooling modules, *Case Studies in Thermal Engineering*, 2020, **18**, 100583, doi: 10.1016/j.csite.2020.100583.
[31] S. Sirikasemsuk, S. Wiriyasart, P. Naphon, N. Naphon, Thermal cooling characteristics of Li-ion battery pack with thermoelectric ferrofluid cooling module, *International Journal of Energy Research*, 2021, **45**, 8824-8836, doi: 10.1002/er.6417.
[32] S. Sirikasemsuk, S. Wiriyasart, R. Prurapark, N. Naphon, P. Naphon, Water/nanofluid pulsating flow in thermoelectric module for cooling electric vehicle battery systems, *International Journal of Heat and Technology*, 2021, **39**, 1618-1626, doi: 10.18280/ijht.390525.
[33] S. Sirikasemsuk, S. Wiriyasart, N. Naphon, P. Naphon, Flow direction effects on Li-ion cylindrical battery management cooling system with water/ferrofluid as coolants, *Frontiers In*

Heat Mass Transfer, 2022, **19**, 1-11, doi: 10.5098/hmt.19.31.
[34] S. Sirikasemsuk, N. Naphon, S. Eiamsa-ard, P. Naphon, Analysis of nanofluid flow and heat transfer behavior of Li-ion battery modules, *International Journal of Heat and Mass Transfer*, 2023, **208**, 124058, doi: 10.1016/j.ijheatmasstransfer.2023.124058.
[35] S. Sirikasemsuk, P. Vengsungnle, S. Eiamsa-ard, P. Naphon, Thermal management of prismatic $LiFePO_4$ battery module with inversed-zigzag channeled ferrofluid flows, *Engineered Science*, 2023, **27**, 1017, doi: 10.30919/es1017
[36] S. Sirikasemsuk, N. Naphon, P. Naphon, Investigation into thermal cooling with different ferrofluid flow arrangements for a lithium-ion battery pack, *Heat Transfer Engineering*, 2024, **45**, 1257-1273, doi: 10.1080/01457632.2023.2249733.
[37] H. Behi, D. Karimi, R. Youssef, M. Suresh Patil, J. Van Mierlo, M. Berecibar, Comprehensive passive thermal management systems for electric vehicles, *Energies*, 2021, **14**, 3881, doi: 10.3390/en14133881.
[38] J. Jaguemont, N. Omar, P. Van den Bossche, J. Mierlo, Phase-change materials (PCM) for automotive applications: A review, *Applied Thermal Engineering*, 2018, **132**, 308-320, doi: 10.1016/j.applthermaleng.2017.12.097.
[39] L. Ianniciello, P. H. Biwolé, P. Achard, Electric vehicles batteries thermal management systems employing phase change materials, *Journal of Power Sources*, 2018, **378**, 383-403, doi: 10.1016/j.jpowsour.2017.12.071.
[40] A. R. M. Siddique, S. Mahmud, B. Van Heyst, A comprehensive review on a passive (phase change materials) and an active (thermoelectric cooler) battery thermal management system and their limitations, *Journal of Power Sources*, 2018, **401**, 224-237, doi: 10.1016/j.jpowsour.2018.08.094.
[41] J. Chen, S. Kang, E. Jiaqiang, Z. Huang, K. Wei, B. Zhang, H. Zhu, Y. Deng, F. Zhang, G. Liao, Effects of different phase change material thermal management strategies on the cooling performance of the power lithium-ion batteries: A review, *Journal of Power Sources*, 2019, **442**, 227228, doi: 10.1016/j.jpowsour.2019.227228.
[42] J. Luo, D. Zou, Y. Wang, S. Wang, L. Huang, Battery thermal management systems (BTMs) based on phase change material (PCM): A comprehensive review, *Chemical Engineering Journal*, 2022, **430**, 132741, doi: 10.1016/j.cej.2021.132741.
[43] Y. Wang, Z. Wang, H. Min, H. Li, Q. Li, Performance investigation of a passive battery thermal management system applied with phase change material, *Journal of Energy Storage*, 2021, **35**, 102279, doi: 10.1016/j.est.2021.102279.
[44] M. Malik, I. Dincer, M. Rosen, M. Fowler, Experimental investigation of a new passive thermal management system for a Li-ion battery pack using phase change composite material, *Electrochimica Acta*, 2017, **257**, 345-355, doi: 10.1016/j.electacta.2017.10.051.
[45] A. Mallow, O. Abdelaziz, S. Graham, Thermal charging performance of enhanced phase change material composites for thermal battery design, *International Journal of Thermal Sciences*, 2018, **127**, 19-28, doi: 10.1016/j.ijthermalsci.2017.12.027.
[46] T. U. Rehman, H. M. Ali, A. Saieed, W. Pao, M. Ali, Copper foam/PCMs based heat sinks: an experimental study for electronic cooling systems, *International Journal of Heat and Mass Transfer*, 2018, **127**, 381-393, doi: 10.1016/j.ijheatmasstransfer.2018.07.120.
[47] A. Arshad, M. Jabbal, Y. Yan, Thermophysical characteristics and application of metallic-oxide based mono and hybrid nanocomposite phase change materials for thermal management systems, *Applied Thermal Engineering*, 2020, **181**, 115999, doi: 10.1016/j.applthermaleng.2020.115999.
[48] M. Pan, W. Lai, Cutting copper fiber/paraffin composite phase change material discharging experimental study based on heat dissipation capability of Li-ion battery, *Renewable Energy*, 2017, **114**, 408-422, doi: 10.1016/j.renene.2017.07.004.
[49] W. Wu, X. Yang, G. Zhang, X. Ke, Z. Wang, W. Situ, X. Li, J. Zhang, An experimental study of thermal management system using copper mesh-enhanced composite phase change materials for power battery pack, *Energy*, 2016, **113**, 909-916, doi: 10.1016/j.energy.2016.07.119.
[50] W. Situ, G. Zhang, X. Li, X. Yang, C. Wei, M. Rao, Z. Wang, C. Wang, W. Wu, A thermal management system for rectangular $LiFePO_4$ battery module using novel double copper mesh-enhanced phase change material plates, *Energy*, 2017, **141**, 613-623, doi: 10.1016/j.energy.2017.09.083.
[51] M. M. Heyhat, S. Mousavi, M. Siavashi, Battery thermal management with thermal energy storage composites of PCM, metal foam, fin and nanoparticle, *Journal of Energy Storage*, 2020, **28**, 101235, doi: 10.1016/j.est.2020.101235.
[52] X. Liu, Z. Rao, Interfacial thermal conductance across hexagonal boron nitride & paraffin based thermal energy storage materials, *Journal of Energy Storage*, 2020, **32**, 101860, doi: 10.1016/j.est.2020.101860.
[53] H. Li, X. Xiao, Y. Wang, C. Lian, Q. Li, Z. Wang, Performance investigation of a battery thermal management system with microencapsulated phase change material suspension, *Applied Thermal Engineering*, 2020, **180**, 115795, doi: 10.1016/j.applthermaleng.2020.115795.
[54] X. Qi, Y. Shao, H. Wu, J. Yang, Y. Wang, Flexible phase change composite materials with simultaneous light energy storage and light-actuated shape memory capability, *Composites Science and Technology*, 2019, **181**, 107714, doi: 10.1016/j.compscitech.2019.107714.
[55] X. Zhang, J. Niu, J. Wu, Development and characterization of novel and stable silicon nanoparticles-embedded PCM-in-water emulsions for thermal energy storage, *Applied Energy*, 2019, **238**, 1407-1416, doi: 10.1016/j.apenergy.2019.01.159.
[56] F. Wang, J. Cao, Z. Ling, Z. Zhang, X. Fang, Experimental and simulative investigations on a phase change material nano-emulsion-based liquid cooling thermal management system for a lithium-ion battery pack, *Energy*, 2020, **207**, 118215, doi: 10.1016/j.energy.2020.118215.
[57] P. Ramadass, B. Haran, R. White, B. N. Popov, Capacity fade of Sony 18650 cells cycled at elevated temperatures Part II. Capacity fade analysis, *Journal of Power Sources*, 2002, **112**, 614-620, doi: 10.1016/S0378-7753(02)00473-1.

[58] L. Liu, X. Zhang, X. Lin, Recent developments of thermal management strategies for lithium-ion batteries: a state-of-the-art review, *Energy Technology*, 2022, **10**, 2101135, doi: 10.1002/ente.202101135.
[59] R. Zhao, J. Gu, J. Liu, Optimization of a phase change material based internal cooling system for cylindrical Li-ion battery pack and a hybrid cooling design, *Energy*, 2017, **135**, 811-822, doi: 10.1016/j.energy.2017.06.168.
[60] A. Lazrak, J. F. Fourmigué, J. F. Robin, An innovative practical battery thermal management system based on phase change materials: Numerical and experimental investigations, *Applied Thermal Engineering*, 2018, **128**, 20-32, doi: 10.1016/j.applthermaleng.2017.08.172.
[61] M. Mehrabi-Kermani, E. Houshfar, M. Ashjaee, A novel hybrid thermal management for Li-ion batteries using phase change materials embedded in copper foams combined with forced-air convection, *International Journal of Thermal Sciences*, 2019, **141**, 47-61, doi: 10.1016/j.ijthermalsci.2019.03.026.
[62] Z. Rao, Q. Wang, C. Huang, Investigation of the thermal performance of phase change material/mini-channel coupled battery thermal management system, *Applied Energy*, 2016, **164**, 659-669, doi: 10.1016/j.apenergy.2015.12.021.
[63] F. Bai, M. Chen, W. Song, Z. Feng, Y. Li, Y. Ding, Thermal management performances of PCM/water cooling-plate using for lithium-ion battery module based on non-uniform internal heat source, *Applied Thermal Engineering*, 2017, **126**, 17-27, doi: 10.1016/j.applthermaleng.2017.07.141.
[64] M. Akbarzadeh, T. Kalogiannis, L. Jin, D. Karimi, J. Van Mierlo, M. Berecibar, Experimental and numerical thermal analysis of a lithium-ion battery module based on a novel liquid cooling plate embedded with phase change material, *Journal of Energy Storage*, 2022, **50**, 104673, doi: 10.1016/j.est.2022.104673.
[65] J. Gou, W. Liu, Y. Luo, The thermal performance of a novel internal cooling method for the electric vehicle battery: An experimental study, *Applied Thermal Engineering*, 2019, **161**, 114102, doi: 10.1016/j.applthermaleng.2019.114102.
[66] Z. Y. Jiang, Z. G. Qu, Lithium–ion battery thermal management using heat pipe and phase change material during discharge–charge cycle: A comprehensive numerical study, *Applied Energy*, 2019, **242**, 378-392, doi: 10.1016/j.apenergy.2019.03.043.
[67] W. Zhang, J. Qiu, X. Yin, D. Wang, A novel heat pipe assisted separation type battery thermal management system based on phase change material, *Applied Thermal Engineering*, 2020, **165**, 114571, doi: 10.1016/j.applthermaleng.2019.114571.
[68] Q. Huang, X. Li, G. Zhang, J. Zhang, F. He, Y. Li, Experimental investigation of the thermal performance of heat pipe assisted phase change material for battery thermal management system, *Applied Thermal Engineering*, 2018, **141**, 1092-1100, doi: 10.1016/j.applthermaleng.2018.06.048.
[69] B. C. Pak, Y. I. Cho, Hydrodynamic and heat transfer study of dispersed fluids with submicron metallic oxide particles, *Experimental Heat Transfer*, 1998, **11**, 151-170, doi: 10.1080/08916159808946559.
[70] Y. Xuan, W. Roetzel, Conceptions for heat transfer correlation of nanofluids, *International Journal of Heat and Mass Transfer*, 2000, **43**, 3701-3707, doi: 10.1016/s0017-9310(99)00369-5.
[71] D. A. Drew, S. L. Passman, Theory of Multicomponent Fluids, New York, NY: Springer New York, 1999, doi: 10.1007/b97678.
[72] J. C. Maxwell, A Treatise on Electricity and Magnetism, Cambridge, UK: Cambridge University Press, 2010, doi: 10.1017/cbo9780511709333.
[73] M. Akbari, N. Galanis, A. Behzadmehr, Comparative analysis of single and two-phase models for CFD studies of nanofluid heat transfer, *International Journal of Thermal Sciences*, 2011, **50**, 1343-1354, doi: 10.1016/j.ijthermalsci.2011.03.008.
[74] M. Kalteh, A. Abbassi, M. Saffar-Avval, A. Frijns, A. Darhuber, J. Harting, Experimental and numerical investigation of nanofluid forced convection inside a wide microchannel heat sink, *Applied Thermal Engineering*, 2012, **36**, 260-268, doi: 10.1016/j.applthermaleng.2011.10.023.
[75] M. Kalteh, A. Abbassi, M. Saffar-Avval, J. Harting, Eulerian–Eulerian two-phase numerical simulation of nanofluid laminar forced convection in a microchannel, *International Journal of Heat and Fluid Flow*, 2011, **32**, 107-116, doi: 10.1016/j.ijheatfluidflow.2010.08.001.
[76] D. A. Drew, R. T. Lahey, Analytical modeling of multiphase flow. In: Roco, MC (Ed.), Particulate two-phase flow, Chapter 6, Butterworth–Heinemann, Boston, 1993, 509-566, ISBN: 0750692758.
[77] J. X. Bouillard, R. W. Lyczkowski, D. Gidaspow, Porosity distributions in a fluidized bed with an immersed obstacle, *AIChE Journal*, 1989, **35**, 908-922, doi: 10.1002/aic.690350604.
[78] N. Wakao, S. Kaguei, Heat and mass transfer in packed beds, New York: Gordon and Breach Science Publishers, 1983, 364, ISBN: 9780677058603.
[79] J. A. M. Kuipers, W. Prins, W. P. M. Van Swaaij, Numerical calculation of wall-to-bed heat-transfer coefficients in gas-fluidized beds, *AIChE Journal*, 1992, **38**, 1079-1091, doi: 10.1002/aic.690380711.
[80] A. Nazari, S. Farhad, Heat generation in lithium-ion batteries with different nominal capacities and chemistries, *Applied Thermal Engineering*, 2017, **125**, 1501-1517, doi: 10.1016/j.applthermaleng.2017.07.126.
[81] D. Bernardi, E. Pawlikowski, J. Newman, A general energy balance for battery systems, Journal of The Electrochemical Society, 1985, **132**, 5-12, doi: 10.1149/1.2113792.
[82] C. Heubner, M. Schneider, C. Lämmel, A. Michaelis, Local heat generation in a single stack lithium-ion battery cell, *Electrochimica Acta*, 2015, **186**, 404-412, doi: 10.1016/j.electacta.2015.10.182.